# Peer-Reviewed Technical Communication

## Multicarrier Acoustic Communications in Multiuser and Interference-Limited Regimes

Zhengnan Li, *Graduate Student Member, IEEE*, and Milica Stojanovic, *Fellow, IEEE*

***Abstract*—In this article, we address the design of a multicarrier communication system based on orthogonal frequency-division multiplexing and direct sequence spread spectrum. The design targets operation in the low-signal-to-noise-ratio regimes and multiuser settings. Specifically, coding is employed across carriers such that channel estimation and signal detection are coupled. We consider both coherent and differentially coherent detection and extend the principles to multichannel reception. A custom-designed frequency synchronization technique is proposed to counteract the motion-induced Doppler frequency shifting effect. Using the recordings from the 2010 Mobile Acoustic Communication Experiment, where signals were transmitted in the 10.5–15.5-kHz acoustic band in shallow water, with relative motion up to 1.5 m/s, we demonstrate the system performance in terms of the mean squared error and bit error rate in data detection. Further employing Polar and low-density parity-check coding, we show that the proposed methods provide excellent performance while maintaining low computational complexity, making them suitable for a practical implementation.**

***Index Terms*—Doppler, low signal-to-noise ratio (SNR), multiuser interference, orthogonal frequency-division multiplexing (OFDM), underwater acoustic communication, underwater networks.**

### I. Introduction

We propose the design of an underwater acoustic communication system capable of operating in multiuser and interference-limited regimes. Multiuser communication enables multiple distributed autonomous underwater vehicles and/or nonmoving assets to exchange information. Multiple access techniques are generally categorized as either random access or deterministic access. While random access is well suited for infrequent and bursty transmissions from multiple spatially distributed users, deterministic access caters to continuous transmissions generated by a fixed number of users. Our focus is on the latter type of scenario, where multiple users communicate via a common base station, which must be capable of simultaneously detecting messages of all the users.

Interference-limited regimes arise in situations with both intentional and unintentional interference. While unintentional interference can be caused by any type of environmental noise, intentional interference is introduced in hostile environments and/or multiuser systems. In addition, in systems that require low probability of detection or intercept, signal levels are deliberately reduced to achieve covert communication, which results in a low signal-to-noise ratio (SNR).

We consider a deterministic access system that is traditionally designed using frequency-division multiple access (FDMA), time-division multiple access (TDMA), or code-division multiple access (CDMA). Each of these methods offers the same theoretical capacity on an additive white Gaussian noise (AWGN) channel, but application scenarios and practicalities (e.g., time synchronization and bandwidth efficiency) may influence the choice of one method over another. Generally speaking, FDMA requires guard bands that limit the bandwidth utilization efficiency. TDMA depends on scheduling such that multiple users' signals arrive to the common receiver in their associated time slots, thus imposing strict demands on synchronization. CDMA and TDMA both offer better multipath diversity than FDMA, while CDMA alone offers a soft capacity limit.

CDMA systems make use of direct sequence (DS) spread spectrum techniques, which are in widespread use in the 3G cellular networks and the global navigation satellite systems. Underwater acoustic CDMA communications have been explored within the general framework of single-carrier and multicarrier broadband modulations. In [1], [2], [3], [4], [5], and [6], the DS spread spectrum in underwater acoustic settings was addressed. In [1], adaptive chip-rate hypothesis-feedback equalization was introduced in the context of single-carrier wideband acoustic communication and demonstrated using field tests. Calvo and Stojanovic [2] explored the problem further from the viewpoint of efficient channel estimation in a multiuser setting. In [3], [4], and [6], spreading code designs were investigated with the goal of alleviating the severe multipath problems introduced by the channels. In particular, He et al. [3] designed a DS spread spectrum system with varying spreading gain that adapts to the channel conditions. A less traditional approach is described in [5], where Liu et al. used dolphin whistles for synchronization and modulated information onto dolphin clicks, verifying the technique in a lake trial.

A competitive alternative to single-carrier communication is multicarrier communication, which is typically implemented by orthogonal frequency-division multiplexing (OFDM) modulation. The major advantages of OFDM systems lie in their bandwidth scalability and low computational complexity achieved through the fast Fourier transform (FFT). The Gaussian-like behavior of OFDM waveforms is a further benefit for covert communications. A variety of signal processing methods for acoustic OFDM have been developed in recent years and successfully demonstrated on real data [7], [8], [9].

Multiuser multicarrier communications based on the DS spread spectrum were investigated heavily in cellular systems (see, e.g., [10]), but remain scarce in underwater acoustic systems. The DS spread spectrum with OFDM (DS-OFDM) for acoustic applications was also considered in [11] and [12], where the authors proposed multiband spread spectrum transceiver designs verified in sea trials. Specifically,

Manuscript received 1 January 2022; revised 25 July 2022; accepted 26 August 2022. This work was supported by the Office of Naval Research under Grant N00014-20-1-2453. An earlier version of this paper was presented at the Global Oceans 2020: Singapore-U.S. Gulf Coast, Oct. 5–30, 2020 [DOI: 10.1109/IEEECONF38699.2020.9389320]. *(Corresponding author: Zhengnan Li.)*

**Associate Editor: K. Pelekanakis.**

The authors are with Northeastern University, Boston, MA 02115 USA (e-mail: li.zhengn@northeastern.edu; millitsa@ece.neu.edu).

Digital Object Identifier 10.1109/JOE.2022.3212826

van Walree et al. [11] used an approach where the entire bandwidth was divided into several subbands, and a single-carrier spread spectrum modulation applied in each subband. Leus and van Walree [12] proposed a time–frequency spreading method and evaluated it using experimental data. This method is based on a multiband OFDM approach, where the total available bandwidth is divided into several subbands, and each subband contains one OFDM stream (e.g., 16 subbands are allocated 256 carriers each). A coded signal is then repeated (spread) over the subbands, as well as over the blocks in time. Coherent detection is employed, with pilots allocated to each subband at an overhead rate of about 50%. Channel estimation utilizes a basis expansion method, while equalization and despreading are performed jointly. Wang et al. [13] employed successive interference cancellation along with iterative sparse channel estimation and low-density parity-check (LDPC) coding. Low bit error rate (BER) results were achieved, in exchange for computational complexity. Iruthayanathan et al. [14] evaluated the performance of a spread-spectrum-based multicarrier system for underwater acoustic communications. The spread spectrum technique is used to mitigate the effects of interference in ambient noise. The authors utilized transmitter precoding in the context of multiuser communications. Egnor et al. [15] explored the possibilities of using frequency hopping spread spectrum technique for multiuser communications. Qiao et al. [16] exploited the nested code structure of the Polar codes. The information bits that belong to each user are placed in the codebook to mitigate the multiuser interference. Such a placement does not depend on successive interference cancellation, thus reducing the complexity of the proposed algorithm. Zakharov and Morozov [17] combined the DS spread spectrum with OFDM, where a binary pseudorandom pilot sequence was modulated on the real part of the quaternary phase-shift keying (QPSK) symbols, and the information bits were modulated on the imaginary part.

In our previous studies [18] and [19], we explored the capabilities of DS-OFDM in underwater acoustic communications. In [18], we investigated the DS-OFDM system in a low-SNR setting, and in [19], we employed DS-OFDM in a multiuser scenario. Here, we build on the principles of [18] and [19] to develop a fully operational system that includes coding across carriers and users, multichannel reception, and signal detection in either coherent or differentially coherent form. We demonstrate the results using real data recorded during the 2010 Mobile Acoustic Communication Experiment (MACE'10), where signals were transmitted in the 10.5–15.5-kHz acoustic band over distances varying from 3 to 7 km and speeds up to 1.5 m/s. We consider an asynchronous uplink system where transmissions from multiple users are not required to arrive synchronously at the receiver. Single-user low-SNR experimental settings are also considered. To account for Doppler shifting, we draw on the ideas of Tadayon and Stojanovic [8] to develop a Doppler frequency synchronization method for the DS-OFDM system. Finally, we employ Polar codes to drive the BER to very low values.

The main contributions of this article are summarized as follows.

1) Within the framework of asynchronous multiuser communication based on DS spread spectrum OFDM modulation, we propose a method in which the process of spreading/despreading is custom designed to suit the propagation channel. By choosing the spreading code to be at least as long as the multipath spread of the channel (as measured in samples), the preprocessing stage of our receiver yields a set of signals that carry different information symbols but depend on the *same* effective channel vector. This fact is exploited to combine the multiple channel observations toward an improved channel estimate and, consequently, improved data detection. Data detection also capitalizes on the fact that individual multipath components are isolated during channel estimation and subsequently combined so as to yield a multipath diversity gain. The process is applicable to any linear modulation, such as phase shift keying (PSK) or quadrature amplitude modulation (QAM).
2) In addition to coherent detection, we present differentially coherent detection that is applicable to the PSK modulation. Both the methods are cast into the multichannel reception framework that exploits spatial diversity.
3) We utilize a frequency offset compensation method that identifies and counteracts the residual frequency offset after resampling.
4) We apply Polar codes and LDPC codes to the proposed system and demonstrate the system performance using real data.

The rest of this article is organized as follows. In Section II, we introduce the signal and system model along with receiver algorithms, highlighting several design considerations. In Section III, we present the results obtained from both the simulations under a statistical underwater channel model, and the experimental signals recorded during MACE'10. Finally, Section IV concludes this article.

## II. System Design Considerations and Signal Detection Methods

We consider an OFDM system with $K$ carriers spanning a bandwidth $B$. The carrier spacing $\Delta f = B/K$ is narrow enough that the channel transfer function appears flat over each subband and sufficiently wide that the channel is constant over the OFDM block duration $T = 1/\Delta f$. These design considerations lead to a system free of intercarrier interference (ICI). We also assume that motion-induced frequency shifting has been properly compensated in an earlier stage of processing (conventional front-end synchronization), such that any residual frequency offsets cause negligible variation over a block duration. OFDM blocks are separated by a guard interval (or cyclic prefix) of length $T_g$, which is at least as long as the delay spread of the channel $T_{mp}$. The guard interval ensures that there is no interblock interference within the system.

In a multiuser system, the transmitted OFDM block of user $u$, $u = 1, \ldots, U$, is given by

$$s_u(t) = \Re\left\{\sum_{k=0}^{K-1} a_{k,u} e^{j2\pi f_k t}\right\}, \qquad t \in [-T_g, T] \tag{1}$$

where $a_{k,u}$ is a coded data symbol of user $u$ modulated onto the carrier $k$ of frequency $f_k = f_0 + k\Delta f$, $k = 0, 1, \ldots, K-1$. If a single-user system only is considered for use in a low-SNR regime, the index $u$ can be omitted. $T_g$ is the guard interval, and $T_g > T_{mp}$.

Following the front-end time and frequency synchronization, FFT demodulation yields the signal observations

$$y_{k,u} = a_{k,u} H_{k,u} + z_{k,u}, \qquad k = 0, 1, \ldots, K-1 \tag{2}$$

where $H_{k,u}$ is the channel transfer function evaluated at carrier $k$ of user $u$, and $z_{k,u}$ represents the noise and any residual multiuser interference.

Data symbols are obtained from a PSK or a QAM alphabet and spread to obtain the transmitted symbols $a_{k,u}$. The spreading gain, i.e., the length of the spreading code, $Q$, is selected such that $Q \geq \lceil BT_{mp} \rceil$. This choice leads to an elegant channel estimation method that is applied to the signal after despreading, thus exploiting the coding gain to improve the channel estimate. To leverage the computational efficiency of FFT, both $Q$ and $K$ are chosen to be a power of 2.

We use binary spreading sequences that can be generated by a pseudorandom generator, maximum-length shift register, or other methods.

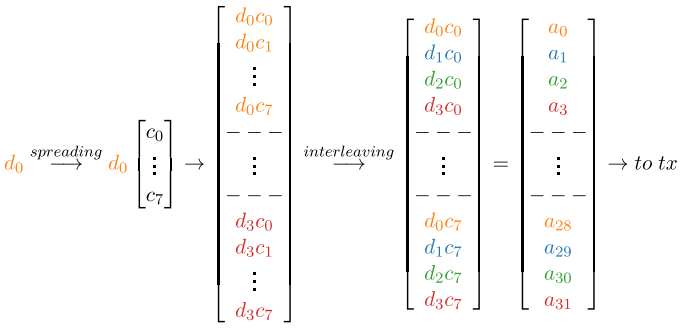


Fig. 1. Spreading process: One data symbol is mapped onto $Q$ chips ($Q = 8$ in this example), with each carrier additionally modulated by the chip of the spreading code. This process is repeated for $I = K/Q$ data symbols ($I = 4$ in this example), and the resulting $K = 32$ coded symbols are interleaved.

For example, Walsh–Hadamard, Gold, and Kasami sequences can be used as the spreading code. In the multiuser scenario, different users are assigned independent spreading sequences, while in the single-user low-SNR scenario, the choice of the spreading code can be arbitrary.

The encoding process for every user begins with mapping $I = K/Q$ information symbols onto $Q$ chips (elements of the spreading sequence), which will eventually lead to $K$ coded symbols per OFDM block. The spreading procedure in a multiuser setting is the same for every user. Denoting user $u$'s spreading sequence as $c_{q,u}$, $q = 0, \ldots, Q-1$, and its $i$th data symbol $d_{i,u}$, $i = 0, \ldots, I-1$, the spreading process is defined by

$$a_{qI+i,u} = d_{i,u} c_{q,u}. \tag{3}$$

This process is illustrated in Fig. 1.

## A. Signal Detection

The signal detection stage of the proposed system begins with despreading according to

$$c^*_{q,u} y_{qI+i,u} = x_{qI+i,u} = d_{i,u} H_{qI+i,u} + c^*_{q,u} z_{qI+i,u} \tag{4}$$

where $(\cdot)^*$ denotes conjugate. If the spreading sequence is binary, conjugation can be omitted.

Arranging these signals into a vector form yields

$$\mathbf{x}_{i,u} = d_{i,u}\mathbf{H}_{i,u} + \mathbf{z}_{i,u}, \qquad i = 0, \ldots, I-1 \tag{5}$$

where $\mathbf{H}_{i,u} = [\ H_{i,u} \quad H_{I+i,u} \quad H_{2I+i,u} \quad \cdots\ ]^\top$ is a $Q$-element channel vector obtained by taking every $I$th element from the full $K$-element channel vector $\mathbf{H}_u = [\ H_{0,u} \quad \cdots \quad H_{K-1,u}\ ]^\top$ beginning with element $i$.

The channel transfer function of user $u$, $\mathbf{H}_u$, is in a discrete Fourier transform (DFT) relationship with an equivalent impulse response $\mathbf{h}_u$, i.e., $\mathbf{H}_u = \mathbf{F}\mathbf{h}_u$, where $\mathbf{F}$ is a proper DFT matrix of size $K \times K$. Because $T > T_{mp}$, the equivalent impulse response will have only $L = \lceil BT_{mp} \rceil \ll K$ significant samples. Consequently, the DFT relationship can equivalently be stated by defining the matrix $\mathbf{F}$ as containing only the first $L$ columns of a proper $K \times K$ DFT matrix, and $\mathbf{h}_u$ as a vector containing only the first $L$ elements of the equivalent impulse response. Note that among the $L$ elements, some can still be negligible as the acoustic channels tend to be sparse.

Substituting the DFT relationship into (5), we have that

$$\mathbf{x}_{i,u} = d_{i,u}\mathbf{F}_i\mathbf{h}_u + \mathbf{z}_{i,u} \tag{6}$$

where $\mathbf{F}_i$ is a $Q \times L$ matrix obtained by taking every $I$th row of the $K \times L$ reduced Fourier matrix $\mathbf{F}$, beginning with column $i = 0, \ldots, I-1$. Multiplying both the sides of the above expressions by $\mathbf{F}'_i$,[1] and recognizing the fact that $\mathbf{F}'_i\mathbf{F}_i = Q\mathbf{I}$ by the virtue of having chosen $Q \geq L$, we obtain

$$\mathbf{u}_{i,u} = \frac{1}{Q}\mathbf{F}'_i\mathbf{x}_{i,u} = d_{i,u}\mathbf{h}_u + \mathbf{w}_{i,u} \tag{7}$$

where $\mathbf{w}_{i,u}$ is the equivalent residual noise.

The signals $\mathbf{u}_{i,u}$ serve as the input to data detection. It is worthwhile pointing out that each of the $I$ signals $\mathbf{u}_{i,u}$, $i = 0, \ldots, I-1$, carries the information about a different data symbol $d_i$, but depends on the *same* channel vector $\mathbf{h}_u$. This fact can be exploited in designing an efficient channel estimator.

In the multiuser setting, $U$ channels need to be estimated, but the procedure followed by each user's channel estimator is the same.

If the channel vectors were known, the data symbols could be estimated in the least squares (LS) manner as[2]

$$\begin{aligned}\hat{d}_{i,u} &= \frac{1}{\|\mathbf{h}_u\|^2}\mathbf{h}'_u\mathbf{u}_{i,u} \\ &= d_{i,u} + \frac{1}{\|\mathbf{h}_u\|^2}\mathbf{h}'_u\mathbf{w}_{i,u}\end{aligned} \tag{8}$$

and the decisions made by finding the nearest valid constellation point $\tilde{d}_{i,u} = \text{dec}\{\hat{d}_{i,u}\}$. In practice, the channel vectors remain unknown. We propose two methods to deal with the unknown channel: one based on coherent detection, and another on differentially coherent detection that is suitable for PSK modulations. Coherent detection relies on explicit channel estimation, while differentially coherent detection, which is used with PSK modulation, sidesteps channel estimation by relying on coherence between adjacent carriers.

*1) Coherent Detection:* To estimate the channel, one of the data symbols in each block is assigned as the pilot, say the first data symbol $d_{0,u}$. LS estimation can now be applied iteratively, yielding the first estimate

$$\hat{\mathbf{h}}_u = \hat{\mathbf{h}}_{0,u} = \mathbf{u}_{0,u}/d_{0,u}. \tag{9}$$

This single-shot channel estimate can be used to estimate the remaining information-carrying data symbols and make the corresponding symbol decisions as

$$\begin{aligned}\hat{d}_{i,u} &= \frac{1}{\left\|\hat{\mathbf{h}}_u\right\|^2}\hat{\mathbf{h}}'_u\mathbf{u}_{i,u} \\ \tilde{d}_{i,u} &= \text{dec}\left\{\hat{d}_{i,u}\right\}.\end{aligned} \tag{10}$$

The procedure is applied individually for each user's channel.

While the approach described above is a simple one, further improvements can be targeted through a refined procedure. Namely, after making the first tentative decision $\tilde{d}_{1,u}$ from the estimates, a new channel estimate is formed as

$$\hat{\mathbf{h}}_{1,u} = \mathbf{u}_{1,u}/\tilde{d}_{1,u}. \tag{11}$$

This estimate is combined with the existing one, $\mathbf{h}_{0,u}$, to form an average, and the procedure then repeats. In other words, every new estimate is obtained as a running average

$$\hat{\mathbf{h}}_{i,u} = (1-\alpha_i)\hat{\mathbf{h}}_{i-1,u} + \alpha_i\mathbf{u}_{i,u}/\tilde{d}_{i,u} \tag{12}$$

where the averaging factors $\alpha_i$ can be chosen as a constant, or as $\alpha_i = \frac{1}{i+1}$, in which case the instantaneous channel estimates are directly averaged as the recursion progresses. The running estimate $\hat{\mathbf{h}}_{i,u}$

[1] $(\cdot)'$ represents the conjugate transpose.

[2] $||\cdot||^2$ denotes the squared norm 2 of a vector.

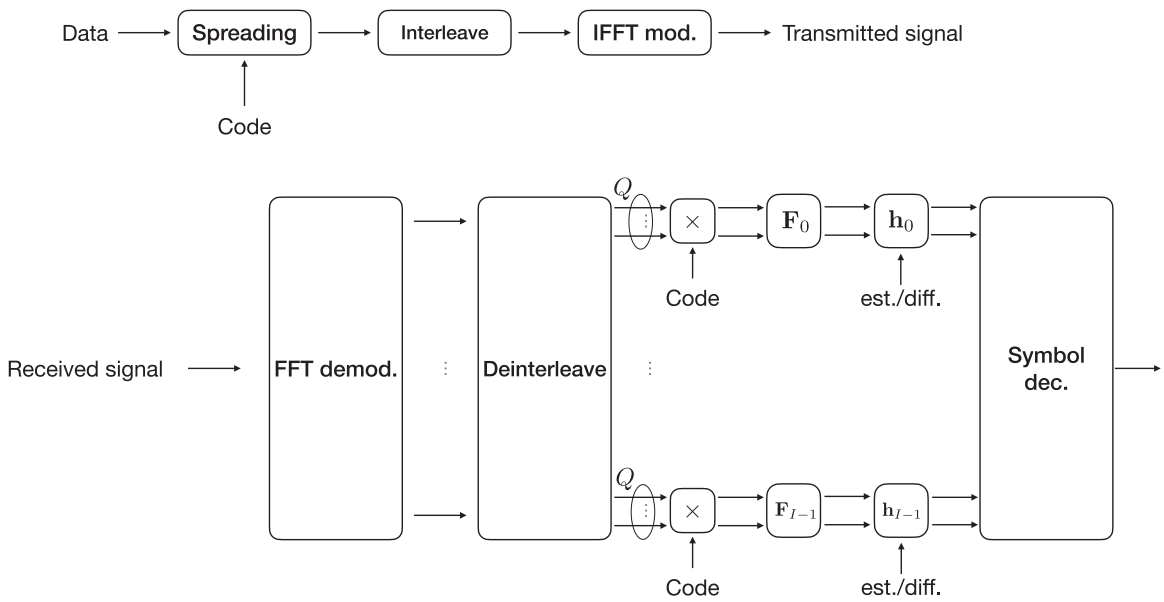


Fig. 2. Block diagram of the DS-OFDM transceiver architecture. The length of the spreading code $Q$ and the number of carriers $K$ correspond to $I = K/Q$ data symbols comprising one OFDM block. Channel estimation is performed with coherent detection, while differentially coherent detection relies on frequency coherence to sidestep the need for channel estimation. In both the cases, frequency-domain equalization is performed after spreading code removal. This figure illustrates a single-input single-output system architecture.

is then used to make the next symbol decision

$$\hat{d}_{i+1,u} = \frac{1}{\left\|\hat{\mathbf{h}}_{i,u}\right\|^2}\hat{\mathbf{h}}'_{i,u}\mathbf{u}_{i+1,u}$$

$$\tilde{d}_{i+1,u} = \mathrm{dec}\left\{\hat{d}_{i+1,u}\right\} \tag{13}$$

and the recursion continues until the last of the $I$ data symbols is detected. Using the final channel estimate, all the data symbols can be re-estimated and final decisions can be made. Note that the data symbol estimation essentially relies on multipath recombining and as such may be regarded as a second stage of despreading, in which the benefits of multipath diversity are exploited in a coherent manner.

The sparsing of the channel estimate can also be applied to eliminate the insignificant channel taps that contribute only noise. We shall comment on sparsing in more detail in Section II-D.

*2) Differentially Coherent Detection:* Differentially coherent detection eliminates the need of channel estimation, relying instead on the coherence between the carriers and differential encoding in the frequency domain. In the context of acoustic OFDM, differentially coherent detection has been addressed in [7] and [9], where it was shown to achieve excellent performance in experimental trials. This fact motivates our proposal of using differentially coherent detection in the multiuser DS-OFDM scenario.

The inputs to the differentially coherent detector are the observations $\mathbf{u}_{i,u}$ given in (7). The transmitted data symbols $d_{i,u}$ are now generated through the differential encoding of the original information-bearing symbols $b_{i,u}$, which is performed as $d_{i,u} = b_{i,u}d_{i-1,u}$. The encoding process begins with a known value of the first symbol, e.g., $d_{0,u} = 1$.

Differentially coherent detection is now performed by making an estimate

$$\hat{b}_{i,u} = \frac{\mathbf{u}'_{i-1,u}\mathbf{u}_{i,u}}{\left\|\mathbf{u}_{i-1,u}\right\|^2} \tag{14}$$

and decisions are made as $\tilde{b}_{i,u} = \mathrm{dec}\{\hat{b}_{i,u}\}$. Note that the signals $\mathbf{u}_i$ and $\mathbf{u}_{i-1}$ contain the *same* channel $\mathbf{h}_u$. Although this channel is unknown, its contribution is canceled in data estimation (14), perfectly when there is no noise and, approximately, when the noise is present.

The system block diagram is shown in Fig. 2.

### B. Multichannel Processing

Spatial diversity reception methods are helpful in cases where one receiving element encounters deep fades, and multichannel reception is often necessary in acoustic systems. We consider the case where the receiver has $M$ receiving elements, and we assume that each receiving element experiences an independently fading channel. This assumption holds when the receiving elements are more than several wavelengths apart from each other. In that case, maximum-ratio combining (MRC) is used in coherent detection, while differential maximum-ratio combining (DMRC) is used in differentially coherent detection.

The signals observed at the $m$th receiver element are now given by

$$\mathbf{u}^m_{i,u} = d_{i,u}\mathbf{h}^m_u + \mathbf{z}^m_{i,u}, \qquad m = 0, \ldots, M-1 \tag{15}$$

where $\mathbf{h}^m_u$ represents the impulse response of the channel corresponding to the element $m$ and user $u$, and $\mathbf{z}^m_{i,u}$ is the noise.

If the noise components are uncorrelated and of equal variance, MRC for coherent detection is performed as

$$\hat{d}_{i,u} = \frac{\sum_{m=0}^{M-1}\hat{\mathbf{h}}^{m'}_{i,u}\mathbf{u}^m_{i,u}}{\sum_{m=0}^{M-1}\left\|\hat{\mathbf{h}}^m_{i,u}\right\|^2}. \tag{16}$$

Analogously, DMRC is performed as

$$\hat{b}_{i,u} = \frac{\sum_{m=0}^{M-1}\mathbf{u}^{m'}_{i-1,u}\mathbf{u}^m_{i,u}}{\sum_{m=0}^{M-1}\left\|\mathbf{u}^m_{i-1,u}\right\|^2}. \tag{17}$$

### C. Frequency Offset Compensation

Our treatment so far assumed that any frequency offset in the received signal has been removed. In practice, motion-induced frequency offset residuals are often present, leading to severe performance degradation if left uncompensated. These residual frequency offsets cause ICI. We

use the principles of [8] to design a super-resolution frequency offset compensation algorithm for the multiuser receiver. The algorithm is based on hypothesizing a range of frequency offsets and performing FFT demodulation under each hypothesis. A selection process is then applied to identify the best hypothesis, and the corresponding frequency offset is used for final demodulation. In the multiuser setting, each user may experience a different frequency offset; therefore, the input signals to the DS-OFDM detector must be synchronized on a per-user basis. Denoting the baseband equivalent of user $u$'s signal received on element $m$ as $v_u^m(t)$, the post-FFT signal on carrier $k$ is given by

$$y_{k,u}^m = \int_T e^{-j\hat{\beta}_u t} v_u^m(t) e^{-j2\pi k\Delta f t} dt \tag{18}$$

where the signal is offset in frequency by a hypothesized value $\hat{\beta}_u/2\pi$. When the receiving elements are co-located, it suffices to use the same estimate $\hat{\beta}_u$ for all the elements $m = 0, \ldots, M-1$.

The signals in (18) are used to detect the data symbols in the same manner as described before. The resulting data symbol estimates $\hat{d}_{i,u}$ and decisions $\tilde{d}_{i,u}$ will depend on the offset estimate $\hat{\beta}_u$. Consequently, by searching through a range of hypothesized values of $\hat{\beta}_u$, the proper frequency offset can be determined as

$$\hat{\beta}_u^\star = \arg\min_{\hat{\beta}_u} \sum_{i=1}^{I-1} \left| \hat{d}_{i,u}(\hat{\beta}_u) - \tilde{d}_{i,u}(\hat{\beta}_u) \right|^2. \tag{19}$$

Once this frequency offset is identified, the final symbol decisions are made as $\tilde{d}_{i,u}(\hat{\beta}_u^\star) = \text{dec}\{\hat{d}_{i,u}(\hat{\beta}_u^\star)\}$.

The procedure is similar for differentially coherent detection, where the frequency offset is estimated as

$$\hat{\beta}_u^\star = \arg\min_{\hat{\beta}_u} \sum_{i=1}^{I-1} \left| \hat{b}_{i,u}(\hat{\beta}_u) - \tilde{b}_{i,u}(\hat{\beta}_u) \right|^2 \tag{20}$$

and the final decisions are made as $\tilde{b}_{i,u}(\hat{\beta}_u^\star) = \text{dec}\{\hat{b}_{i,u}(\hat{\beta}_u^\star)\}$.

### D. Channel Sparsing

Additional improvement in performance can be obtained through channel sparsing. Namely, if it is known that the channel vector $\mathbf{h}_u^m$ exhibits a sparse structure, certain elements of the estimate $\hat{\mathbf{h}}_u^m$ will be discarded. Specifically, those elements ("taps") whose magnitude falls below a certain threshold, $\eta \cdot \max\{|\hat{\mathbf{h}}_{i,u}^m|\}$, can be set to zero. It is worth pointing out that we do not perform thresholding during the iterative process described in (12), but only on the final channel estimate. If thresholding were performed in each iteration, taps that should pass the threshold could be buried in multiuser interference (or noise). However, these taps are likely to persist after averaging. The thresholding process is, thus, performed at the end of recursion, per data symbol $i$ per user $u$ before MRC.

As for differentially coherent detection, sparsing follows the same steps as before, now applied to the signal vectors $\mathbf{u}_{i,u}$, which are sparsed to retain only those elements whose magnitude exceeds the threshold $\eta \cdot \max\{|\mathbf{u}_{i,u}^m|\}$. Sparsing is performed before DMRC, i.e., for each data symbol $i$ and each user $u$, the $\mathbf{u}_{i,u}^m$ is sparsed for every receiving element $m$.

### E. Channel Coding

*1) LDPC Codes:* LDPC codes were proposed by Gallager [20] in 1962. These codes are capacity-approaching codes. The LDPC codes are block codes with parity-check matrices containing only a very small number of nonzero entries. The sparseness guarantees a linear decoding complexity. In this article, we use the parity matrix generation method for arbitrary code rate, described in [21]. With the help from the library in [22], we use the belief propagation with vertical layered scheduling method [23] in conjugation with the sum–product algorithm [21] to decode the systematically encoded LDPC codes. We feed the decoder with the log-likelihood ratios that are calculated using the method proposed in [24].

*2) Polar Codes:* Polar codes were proposed by Arikan [25] in 2008. These codes are the first family of error-correcting codes, which achieves the capacity of binary-input memoryless and symmetric AWGN channels. Efficient encoding and decoding methods for Polar codes have been documented in [26]. Owing to their excellent performance, Polar codes are used for control channel coding in 5G cellular systems [27]. In this article, we employ an efficient Polar code list decoder, which exploits the cyclic redundancy check (CRC) to reduce decoding complexity [26]. The CRC polynomial is described in [27]. From the library given in [22], we utilize the channel reliability index from [27, Table 5.3.1.2-1], which translates to the frozen bits of the Polar encoder, a 16-bit CRC described in [27, Sec. 5.1], a systematic Polar encoder, and the list decoder described in [26]. The length of the list is 8. We feed the decoder with the log-likelihood ratios that are calculated using the method proposed in [24].

While LDPC and Turbo codes outperform Polar codes on an AWGN channel in general, the use of CRC in conjunction with list decoding reverses the situation: Tal and Vardy [28] reported that at lengths 512 and 1024, Polar codes with list decoding perform better than any code currently known when considering a fixed target error probability. In our implementation, Polar codes are used with CRC and list decoding.

### F. Complexity Analysis

The step described by (5) requires $Q$ complex operations, and (7) requires $L \times Q$ operations. If coherent detection is used, the channel estimation step [(9) or (12)] requires $L$ operations. If differentially coherent detection is used, (14) requires $L$ operations. These operations, i.e., (5), (7), (12), or (14), are repeated for all $M$ receivers and all $I$ data symbols. The MRC or the DMRC requires $L^2 \times M$ operations. Therefore, the computational complexity is $\mathcal{O}(M \times L \times Q \times I + L^2 \times M)$. In general, $L \ll K$ and $K = Q \times I$, and the total operation is upper bounded by $\mathcal{O}(M \times L \times K)$. If the frequency offset compensation is used and iterates $N$ times, the overall complexity is $\mathcal{O}(N \times M \times L \times K)$.

## III. Results

### A. 2010 Mobile Acoustic Communication Experiment

The MACE'10 experiment was conducted off the coast of Martha's Vineyard, Massachusetts. In this experiment, a vertical hydrophone array with 12 elements separated by 12 cm recorded signals from a mobile transmitter. The transmitter moved at varying lateral speed up to 1.5 m/s. The hydrophone array was deployed at approximately 40-m depth. All the OFDM signals were transmitted in the 10.5–15.5-kHz acoustic band. A total of 52 transmissions were recorded over 3.5 h, where each transmission contained OFDM signals with $K = 2^7, 2^8, \ldots, 2^{11}$ QPSK-modulated data symbols. The signal set contains two different categories of signals: one with zero-padding and another with cyclic prefix in the guard interval between the OFDM blocks. We use the cyclic prefix version of the signals to demonstrate the proposed system performance. The frame structure of the cyclic prefix OFDM (CP-OFDM) transmitted during the MACE'10 experiment is shown in Fig. 3. In addition, the MACE'10 signal parameters and DS-OFDM system information are listed in Table I, and the ship trajectory is shown in Fig. 4. The experimental data were recorded in the presence of motion, which results in significant frequency shifting.

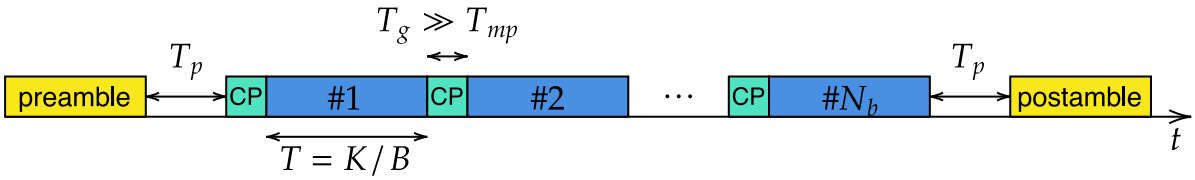


Fig. 3. Frame structure of the CP-OFDM that was transmitted during the MACE'10 experiment. The preamble and the postamble are $2^7 - 1$ bit pseudorandom sequences. The guard interval $T_g$ is 16 ms and the pause period $T_p$ is 32 ms. Eight $K = 1024$ blocks ($N_b = 8$) per location were transmitted, and there were 52 locations in the MACE'10.

TABLE I
MACE'10 SIGNAL PARAMETERS

| number of carriers | 128 | 256 | 512 | 1024 | 2048 |
|---|---|---|---|---|---|
| number of blocks per frame | 64 | 32 | 16 | 8 | 4 |
| carrier spacing [Hz] | 39.1 | 19.5 | 9.8 | 4.9 | 2.4 |
| chip rate $\frac{B}{1+BT_g/K}$ [kb/s] | 6.13 | 7.6 | 8.67 | 9.27 | 9.6 |

The signal bandwidth is $B = 5$ kHz, starting with the lowest carrier frequency $f_0 = 10.5$ kHz. The guard interval $T_g$ is 16 ms and the pause period is $T_p$ is 32 ms.

TABLE II
UNDERWATER ACOUSTIC SIMULATION PARAMETERS

| bandwidth [kHz] | 5 |
|---|---|
| lowest carrier frequency [kHz] | 10.5 |
| center frequency [kHz] | 13 |
| number of carriers $K$ | 1024 |
| water depth [m] | 100 |
| tx–rx distance [km] | 3–6 |
| transmitter depth [m] | 55 |
| receiver depth [m] | 40–41.2 |
| mean of intrapath amplitudes | 0.025 |
| variance of intrapath amplitudes | $10^{-6}$ |
| variance of surface variations | 1.125 |
| variance of bottom variations | 0.5625 |
| number of intra-paths | 20 |

The front-end compensation of the gross frequency offset is performed, as described in [8]. Specifically, frame synchronization is performed by cross-correlating the received signal's preamble with the known synchronization probe (a high-resolution pseudorandom sequence), and a coarse estimate of the Doppler scaling factor is made by measuring the time between the synchronization preamble and the postamble. Front-end resampling is then performed based on the so-obtained estimate. To estimate the residual frequency offset, we hypothesize the frequency offset $\hat{\beta}/2\pi$ in the range $[-3\Delta f, 3\Delta f]$ with resolution $\Delta f/20$. The multipath spread observed in the recorded signals is around 7 ms. In accordance with this value, and with the system bandwidth of 5 kHz, the spreading factor $Q > \lceil B \times T_{mp} \rceil = 35$ suffices for channel estimation.

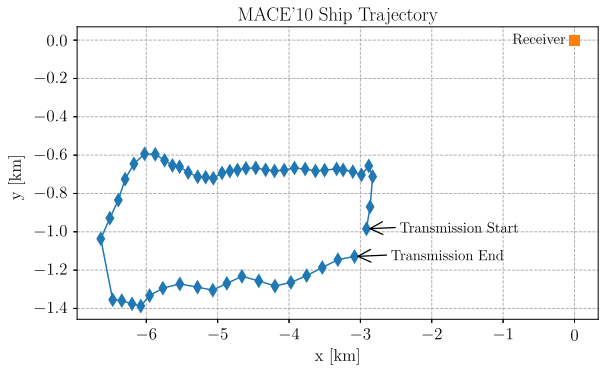


Fig. 4. Ship trajectory of the MACE'10 experiment. The speed of the transmitter varies from 0.5 to 1.5 m/s. The total duration of transmission is 3.5 h, in which 52 transmissions are made at evenly spaced intervals of time, one every 4 min.

Before we move on to the experimental data results, we first present the results of simulation, whose parameters are set to match those of the experiment.

### B. Simulation Results

In this section, we assess the performance of DS-OFDM systems through simulation. We employ the BELLHOP ray tracer [29] to obtain the nominal multipath arrivals for a given bathymetry, sound-speed profile, and signal frequency corresponding to the MACE setup.

To model the underwater acoustic channels more accurately, we add random channel fluctuations and motion-induced Doppler effects using the statistical channel simulator based on [30]. Specifically, we feed the nominal arrivals to the statistical channel simulator to generate random channel realizations that reflect the true underwater channels. The simulation parameters are summarized in Table II. The interested readers are referred to [30] for detailed explanation of the statistical parameters.

The sound-speed profile captured in the MACE experiment and the incoherent acoustic transmission loss simulated through BELLHOP are shown in Fig. 5. A realization of simulated underwater acoustic channel is shown in Fig. 6. Note the presence of shadow zones that the receiver may encounter, resulting in a very low SNR scenario.

To evaluate the DS-OFDM system performance in a multiuser scenario, we emulate uplink multiple access. A $U$-user environment is created by superimposing interfering signals asynchronously transmitted from a selection of $U - 1$ of 52 possible locations onto the target user's signal. These locations are sampled from the MACE'10 transmitter locations. Input signal to the $m$th receiving element is generated as

$$v_m^u(t) = e^{j\beta_u t} \sum_u \sum_k a_{k,u} H_{k,u}^m e^{j2\pi k \Delta f (t-\tau_u)} + w_u^m(t) \qquad (21)$$

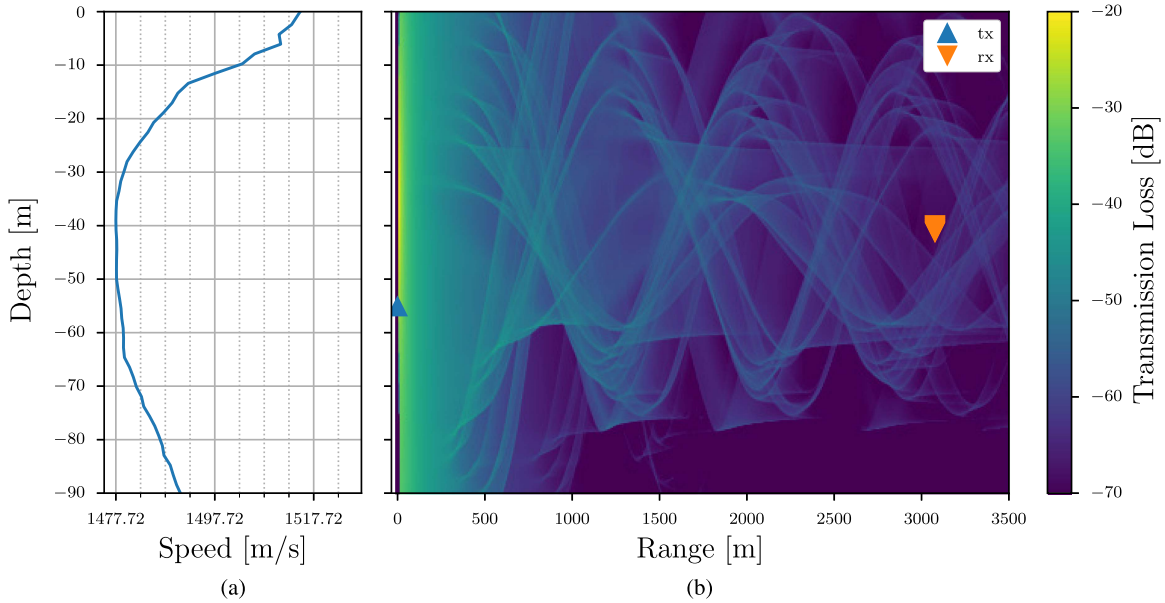


Fig. 5. (a) Sound-speed profile and (b) BELLHOP ray trace beam (incoherent acoustic transmission loss). The soft seabed boundary is modeled as an acoustic elastic half-space having a sound speed of 1400 m/s and density of 1.8 g/cm$^3$. The distance between the transmitter and the receiver is 3 km, matching the first recording of MACE'10.

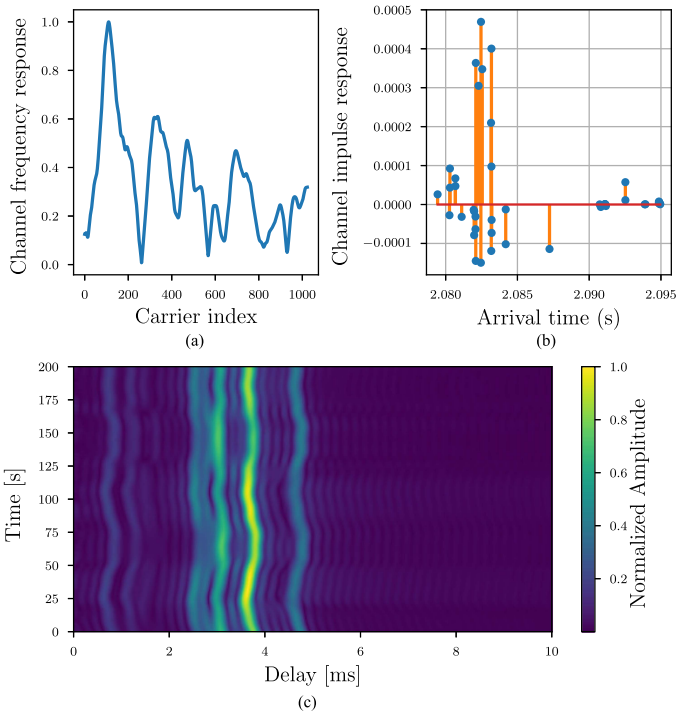


Fig. 6. (a) Channel frequency response for one receiver element. (b) Multipath arrivals generated by BELLHOP. (c) The channel impulse response simulated using the statistical fading model [30]. Only the first 10 ms of the channel response are plotted as the rest is negligible. Frequency shifting due to motion would cause path drifting in time; this is not shown as it is compensated by front-end resampling.

where $w_m^u(t)$ is the equivalent baseband noise, $H_{k,u}^m$ is the channel frequency response generated based on the statistical model [30], and $\tau_u$ is the delay corresponding to user $u$. Note that the users are not assumed to be synchronous, i.e., their delays are different. The SNR in the simulation is 20 dB.

We present the multiuser performance results in Fig. 7(a). To arrive at statistically stable results, we generate 1000 frames for each of the 52 different locations. The number of users is varied from $U = 2$ to 8, and there are $M = 12$ receiving elements. Mean squared error (MSE) results are averaged across Monte Carlo simulations, locations, and frames. Results show very good performance, confirming the viability of the method proposed. Coherent detection is seen to perform better than differentially coherent detection by a margin of 5 dB or more. As expected, the performance improves with increasing spreading gain $Q$, gaining about 3 dB with every doubling of $Q$ with both coherent and differentially coherent detection. Note that when $Q = 32$, coherent detection fails to properly detect the data symbols, which is explained by the fact that the condition $Q > BT_{mp}$ is violated. The BER results are shown in Fig. 7(b).

### C. Experimental Results

We now turn to the discussion of experimental results, addressing first the effects of the MRC and DMRC, subsequently the multiuser scenario, and finally the low-SNR scenario.

*1) Effects of the Multichannel Combining:* In this section, we apply the multichannel combining (16) and (17) to the MACE'10 recordings and demonstrate their performance in terms of the measured MSE in data detection. The MSE is obtained by averaging all 52 OFDM frames, each containing eight blocks. The MSE is shown in Fig. 8. As we can observe from the plot, the performance improves as the array size grows, but exhibits the effect of diminishing returns due to the finite apertures, which indicates that correlation between the elements is introduced.

*2) Multiuser Scenario:* We assume that the power control is in place, as in any multiuser system. Such an assumption ensures that multiple users' signals arrive to the receiver at approximately the same power level. There are various methods for power control available, and we outlined one of such methods in our previous work [31], where we demonstrated the uplink and the downlink multiuser DS-OFDM system using an over-the-air acoustic communications testbed.

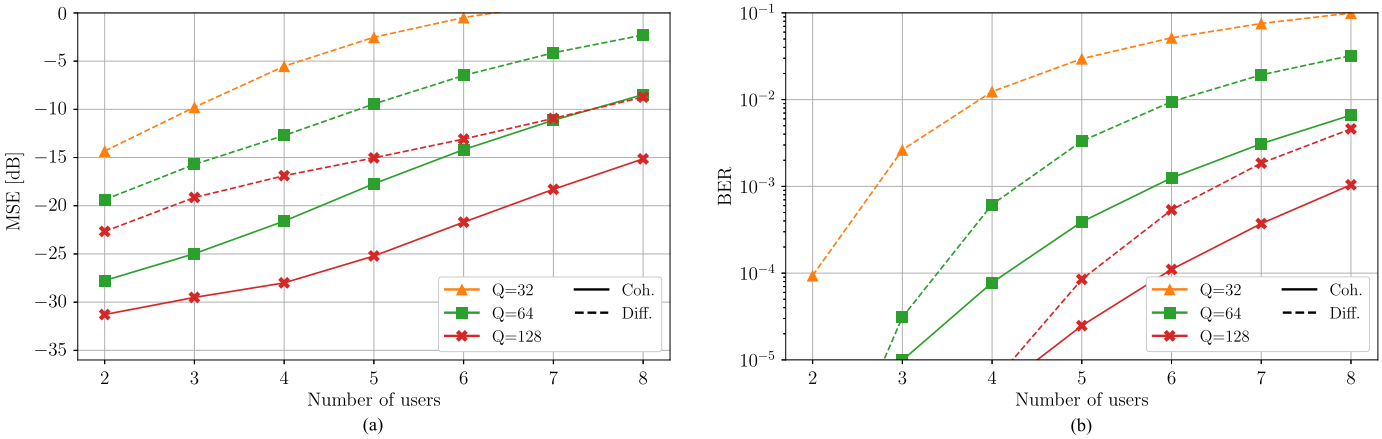


Fig. 7. System performance in terms of estimated MSE and BER. The number of carriers $K = 1024$ and $M = 12$ receiving elements are used to exploit the benefits of MRC. The SNR in the simulation is 20 dB. (a) Estimated MSE in the simulated channel. (b) Estimated BER in the simulated channel.

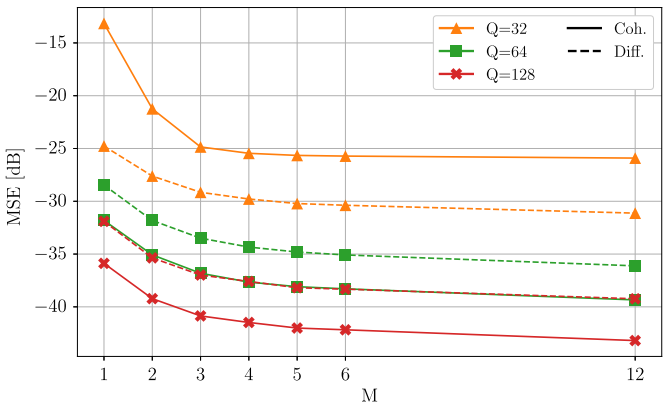


Fig. 8. MSE versus number of receivers. The number of carriers is $K = 1024$. The results are obtained by averaging all 52 OFDM frames and all blocks. Note that the receiver channels are selected such that their spacing is maximized. For instance, if $M = 3$, the receiver spacing is $4 \times 0.12$ m.

To assess the system performance in a multiuser setting, we superimpose individual signals transmitted from different locations. To be specific, we pick $U - 1$ recordings uniformly at random among the 52 transmission locations, normalize their powers to 1 W and add them onto the target user's signal whose power is also normalized to 1 W. Such a process is repeated for all 52 recordings, from which the target user's signal is chosen. The sum signal is then used to emulate $U$ users in an uplink multiaccess scenario. To guarantee fairness for comparison in terms of the number of data symbols $I$, we repeat the process proportionally to the spreading gain, i.e., 1000 times when $Q = 32$, 2000 times when $Q = 64$, and 4000 times when $Q = 128$. The multiuser signals are added in a completely asynchronous manner to mimic a practical underwater acoustic setting where having the different users' signal arrive at the receiver at exactly the same time would be difficult if not impossible. In a practical setting, different users would be assigned different (orthogonal) synchronization preambles, and the processing of a desired user's signal would begin by acquiring its timing from the corresponding cross-correlation peak.

Fig. 9(a) demonstrates the DS-OFDM multiuser system performance in terms of the measured MSE in data detection. Each value of the MSE is obtained by averaging over all 52 recordings, all Monte Carlo realizations per recording, all blocks, and all $I - 1$ data symbols per block. The number of carriers is $K = 1024$, and all $M = 12$ receiving elements are enabled. The processing gain varies from $Q = 32$ to $Q = 128$. One data symbol is used as the pilot, leaving between 31 and 7 information-bearing data symbols per OFDM block, respectively. The performance improves with an increase in the processing gain, offering a range of operation regions. The MSE decreases by 3 dB for every doubling of the processing gain $Q$. For example, with $Q = 32$, the output MSE of $-13$ dB is sustained with six users when the coherent receiver is employed. When the differentially coherent receiver is used, the system is able to support five users with the output MSE of $-13$ dB. Note that in the multiuser setting, the effective signal-to-interference-and-noise ratio (SINR) is below 0 dB. This phenomenon can also be observed in single-user low-SNR results on which we will comment later.

BER results for this scenario are shown in Fig. 9(b). Note that the BER is averaged over all 52 OFDM transmissions, all $2I - 2$ data bits per OFDM block, and all Monte Carlo realizations. These uncoded BER results confirm the observations made from Fig. 9(a): a coherent detector with a spreading gain $Q = 32$ is able to detect data symbols at a BER lower than $10^{-3}$ when there are up to six users. For differentially coherent detection, the DS-OFDM method is able to maintain the same BER level when there are up to five users present in the system. Higher processing gain supports more users at the expense of a reduced data rate. We summarized our recommended settings for an uncoded DS-OFDM system in Table III.

The results presented so far show the average performance in terms of the data detection MSE and BER, both of which are in fact random variables, changing from one time of transmission to the next. To fully assess their statistical behavior, we measure their cumulative distribution function (CDF). Fig. 10(a) and (b) shows the detailed CDF plots of multiuser coherent detection and differentially coherent detection performance, respectively. In both the plots, we can observe that when the number of users doubles, estimated MSE worsens by 3 dB because the SINR drops by about 3 dB, e.g., in Fig. 10(a), when $U = 2$, 80% of the data symbol estimates have the MSE lower than $-29$ dB, while for $U = 3$, 80% of the data symbol estimates show the MSE lower than $-26$ dB. Similar trends can also be seen upon comparing $U = 3$ and $U = 5$ cases, in which the estimated MSE is lower than $-26$ and $-23$ dB, respectively. Furthermore, the trend of these MSE CDF curves matches those of simulations, providing a strong validation of the simulation and the statistical channel simulator itself.

Fig. 11 shows the performance of the DS-OFDM system with channel sparsing at various values of the threshold $\eta$, as we described in Section II-D. The number of carriers is $K = 1024$ and the processing

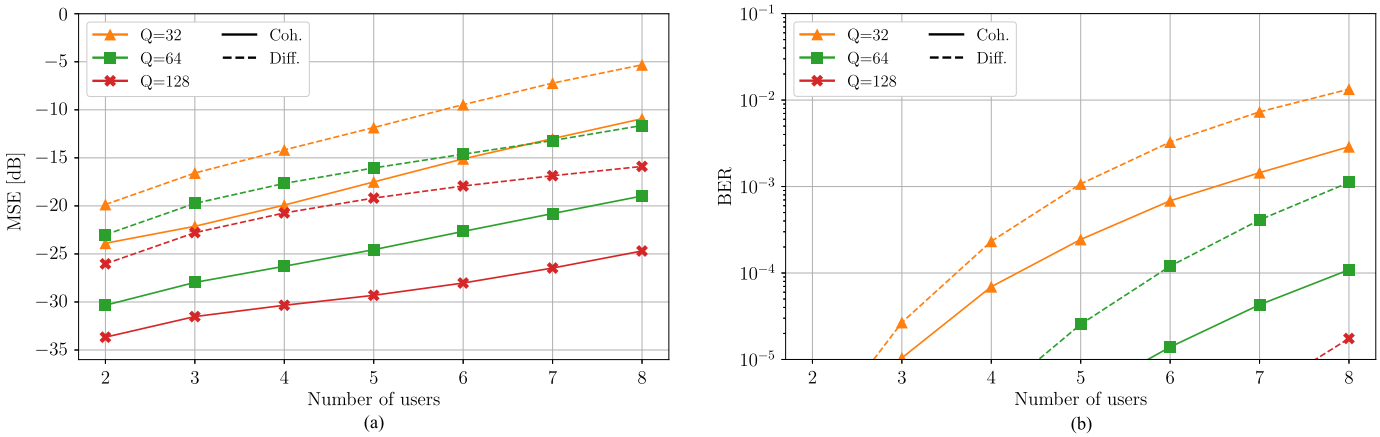


Fig. 9. Estimated symbol MSE and BER versus the number of users, for $K = 1024$ carriers, $M = 12$ receiving elements, and a varying processing gain $Q$. During MACE'10 experiment, the distance between the transmitter and the receiver array varied from 3 to 7 km. The SNRs of the recordings are at or above 20 dB. The results are obtained through averaging over all 52 transmissions, all $I - 1$ data symbols ($2I - 2$ data bits), and all Monte Carlo realizations. (a) Estimated MSE versus the number of users. (b) Estimated BER (uncoded) versus the number of users.

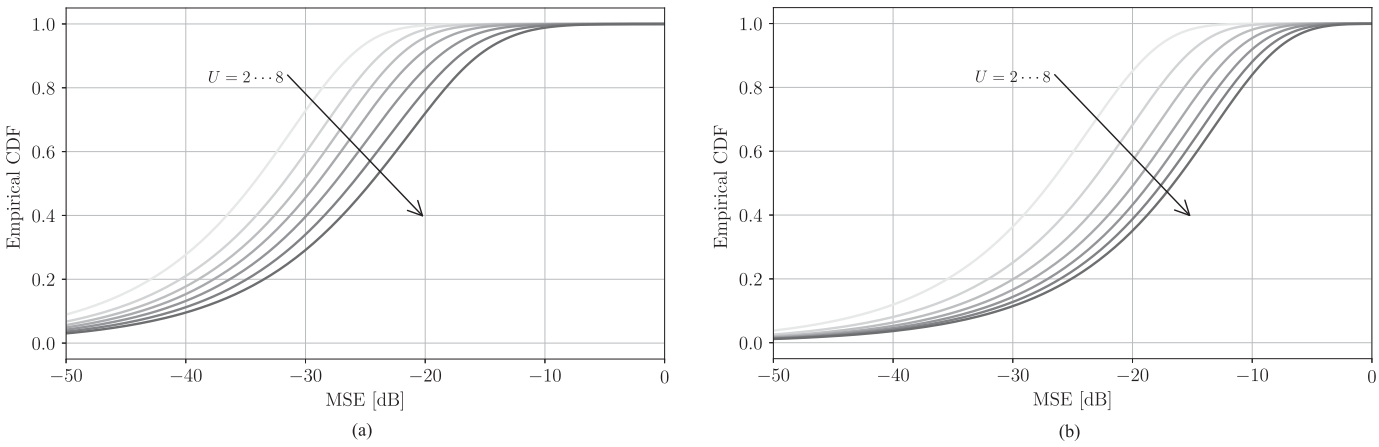


Fig. 10. Cumulative distribution plot of the MSE, with $K = 1024$ carriers, $Q = 64$ spreading gain, and $M = 12$ receiving elements. The results are obtained through averaging over all 52 transmissions, all $I - 1$ data symbols, and all Monte Carlo iterations. (a) Empirical CDF of the estimated MSE, coherent detection. (b) Empirical CDF of the estimated MSE, differentially coherent detection.

TABLE III
RECOMMENDED SETTING FOR AN UNCODED MULTIUSER DS-OFDM SYSTEM

| Target BER | $U$ | $Q$ | Detection | Target BER | $U$ | $Q$ | Detection |
|---|---|---|---|---|---|---|---|
| $10^{-4}$ | 2 | 32 | Both | $10^{-5}$ | 2 | 32 | Both |
| | 3 | 32 | Both | | 3 | 32 | Coherent |
| | 4 | 32 | Coherent | | 4 | 64 | Both |
| | 5 | 64 | Both | | 5 | 64 | Coherent |
| | 6 | 64 | Both | | 6 | 64 | Coherent |
| | 7 | 64 | Coherent | | 7 | 128 | Both |
| | 8 | 64 | Coherent | | 8 | 128 | Coh. |

Recommended minimal (in terms of the spreading gain $Q$) settings for an uncoded DS-OFDM system. The number of carrier is $K = 1024$ and the number of receivers is $M = 12$.

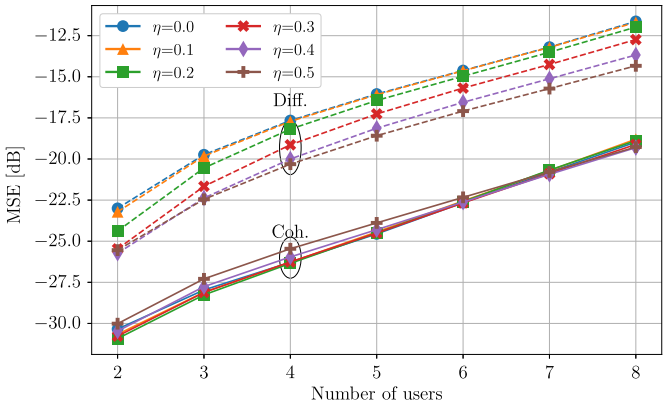


Fig. 11. Measured symbol MSE versus the number of users of the thresholding method. The number of carriers is $K = 1024$, and all $M = 12$ receiving elements are enabled. The processing gain is $Q = 64$. The results are obtained through averaging over all 52 transmissions, all $I - 1$ data symbols ($2I - 2$ data bits), and all Monte Carlo realizations.

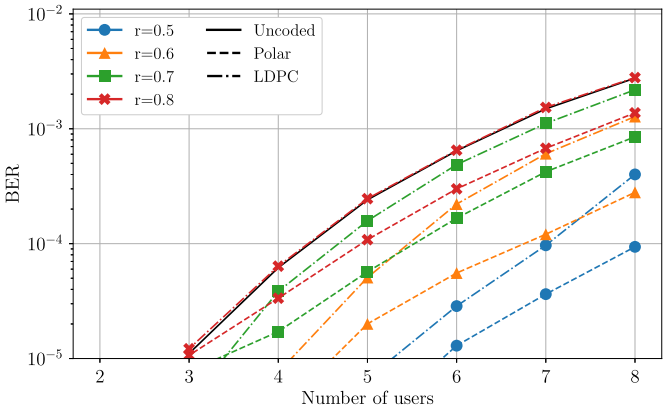


Fig. 12. Measured BER when coherent detection along with Polar code or LDPC code is used. The number of carriers is $K = 1024$. The code rate $r$ is defined as the ratio between the number of information-bearing bits and the number of coded bits. The spreading gain is $Q = 32$ and the codeword length is 512. The results are averaged across all the transmissions and all the simulation realizations. The BER curves corresponding to the Polar codes are shown in dashed-dotted style, and in dashed style for LDPC.

gain is $Q = 64$. All $M = 12$ receivers are enabled. The benefits of sparsing are notably pronounced with differential detection. There, the performance improves by full 2 dB as the threshold $\eta$ increases from 0 (no sparsing) to 0.5. This result is particularly encouraging as the computational complexity of the underlying processing is very low. Note that increasing the threshold $\eta$ above some limit will eventually lead to the elimination of useful taps. A close inspection of coherent detection performance reveals that this effect occurs as $\eta$ increases from 0.4 to 0.5.

We further explore DS-OFDM system performance when Polar codes or LDPC are used. The information bits are coded, and a 16-bit CRC is attached. MACE'10 recordings contain 52 frames with eight OFDM blocks per frame. Thus, when the spreading gain is $Q = 32$ and there are $K = 1024$ carriers, the effective throughput is 256 QPSK data symbols per frame. These QPSK symbols correspond to 512 data bits. With a code rate of 0.5, 256 data bits and a 16-bit CRC are fed to the Polar encoder, which thus contain 240 information bits. When the LDPC codes are used, no CRC is attached.

TABLE IV
RECOMMENDED SETTINGS FOR A POLAR-CODED MULTIUSER DS-OFDM SYSTEM

| Target BER | $Q$ | $U$ | $r$ | Target BER | $Q$ | $U$ | $r$ |
|---|---|---|---|---|---|---|---|
| $10^{-4}$ | 32 | 2 | 1 | $10^{-5}$ | 32 | 2 | 1 |
| | | 3 | 1 | | | 3 | 1 |
| | | 4 | 1 | | | 4 | 0.6 |
| | | 5 | 0.8 | | | 5 | 0.7 |
| | | 6 | 0.6 | | | 6 | 0.5 |
| | | 7 | 0.5 | | | 7 | x |
| | | 8 | 0.5 | | | 8 | x |
| | 64 | 2 | 1 | | 64 | 2 | 1 |
| | | 3 | 1 | | | 3 | 1 |
| | | 4 | 1 | | | 4 | 1 |
| | | 5 | 1 | | | 5 | 1 |
| | | 6 | 1 | | | 6 | 1 |
| | | 7 | 1 | | | 7 | 0.8 |
| | | 8 | 1 | | | 8 | 0.8 |

Recommended settings for a Polar-coded DS-OFDM system. The number of carrier is $K = 1024$ and the number of receivers is $M = 12$. When $r = 1$, no coding is needed. x stands for not achievable with the current selection of parameters.

Fig. 12 shows the performance results of applying coherent detection and Polar codes in a multiuser underwater acoustic communication scenario. The number of carriers is $K = 1024$. The number of realizations in this case is 2000 and the spreading gain is $Q = 32$. This is to guarantee statistically meaningful results at the BER of $10^{-5}$. The results clearly show superior performance of the coded system, either using Polar codes or using the LDPC codes. As expected, when the code rate $r$ decreases, the system has fewer bit errors at the expense of a lower information throughput. Nonetheless, excellent performance is observed. For instance, with a spreading gain of 32, the BER is below $10^{-4}$ with six users, and a Polar code rate of 0.6. These numbers are very encouraging from the standpoint of a practical implementation. The benefits of channel codes are not only in their ability to reduce the bit errors to some degree but also in the fact that they provide a fine tradeoff between the desired number of users and the target BER. By tuning the code rate $r$, a system designer can achieve the desired tradeoff that caters to the specific needs of the system at hand. It is also interesting to note that the Polar code enables successful operation with $Q = 32$ and coherent detection and overcomes insufficient number of channel estimation pilots presented by $Q = 32$. We summarize the recommendations of the parameters in Table IV, when Polar codes are used. For example, if the spreading gain is $Q = 32$ and the number of user is $U = 5$, a Polar code with rate $r = 0.8$ is required to achieve the target BER of $10^{-4}$.

*3) Single-User Low-SNR Scenario:* In this section, we consider a single-user case in which the communication link is to be established in a low-SNR regime. To simulate the underwater acoustic noise, we abstract its frequency characteristics as well as its spatial correlation properties from the pause period in the MACE'10 data and generate

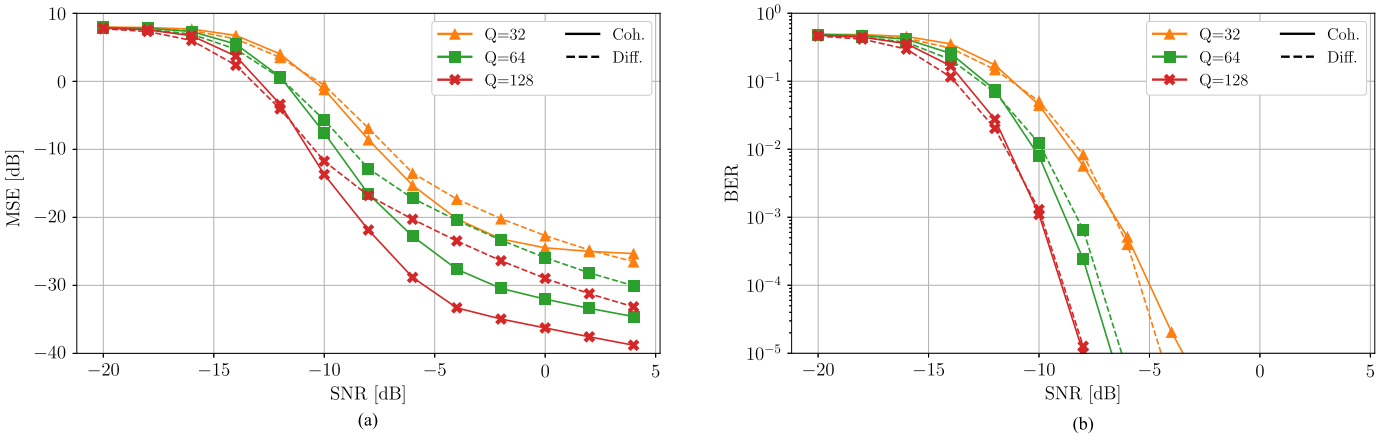


Fig. 13. DS-OFDM system performance in the low-SNR scenario. The number of carriers is $K = 1024$. The results are averaged across 52 transmissions, all $I - 1$ symbols ($2I - 2$ bits) and all the iterations. The background SNR of MACE'10 is 20 dB and omitted. (a) Measured MSE versus SNR. (b) Measured BER versus SNR.

TABLE V
RECOMMENDED SETTINGS FOR AN UNCODED SINGLE-USER DS-OFDM SYSTEM

| | Target BER | $Q$ | SNR [dB] |
|---|---|---|---|
| Coh. | $10^{-4}$ | 32 | −5 |
| | | 64 | −7.5 |
| | | 128 | −9 |
| | $10^{-5}$ | 32 | −4 |
| | | 64 | −7 |
| | | 128 | −8 |
| Diff. | $10^{-4}$ | 32 | −5 |
| | | 64 | −7 |
| | | 128 | −9 |
| | $10^{-5}$ | 32 | −5 |
| | | 64 | −6 |
| | | 128 | −8 |

Recommended minimal (in terms of the SNR) settings for a Polar-coded DS-OFDM system. The number of carrier is $K = 1024$ and the number of receivers is $M = 12$.

the noise according to those statistics. The purpose of this analysis is to validate the system performance under the low-SNR scenario, as well as to provide a cross-validation with the multiuser scenario, in which the asynchronous multiuser interference essentially represents an elevated level of the noise.

Fig. 13 summarizes the system performance in the low-SNR regime. As we observe from Fig. 13(a), coherent detection outperforms the differentially coherent detection when effective SNR is below 0 dB. To compare these results with the multiuser system, let us focus, for example, on the case with $U = 2$ users (the SINR is then around 0 dB, assuming that the noise is negligible as compared to the interfering user's signal), and the spreading gain $Q = 128$, in which the estimated MSE is around $-35$ dB [see Fig. 9(a)]. The same result can be observed in Fig. 13(a). Similarly, when $U = 5$ (the SINR is around $-6$ dB) and $Q = 64$, the estimated MSE in Fig. 9(a) is $-25$ dB, which matches the MSE observed in Fig. 13(a). We summarized the recommended settings for an uncoded single user DS-OFDM system in Table V. For instance, the DS-OFDM system can operate in an SNR of $-5$ dB when $Q = 32$ and the target BER is $10^{-4}$.

## IV. CONCLUSION

In this article, we addressed the problem of multicarrier signal detection in acoustic systems where multiple asynchronous users operate simultaneously in the same band (multipoint-to-point), or in point-to-point links operating in the low-SNR regime. We coupled DS spread spectrum with OFDM in a way that exploits both the necessary processing gain to deal with low signal levels or multiuser interference and efficient channel estimation for coherent data detection. Differentially coherent detection was also considered as a low-complexity alternative to coherent detection. Multichannel combining, along with a custom-designed frequency offset compensation method, and Polar codes were employed to cater to the needs of mobile acoustic systems. Results of both simulation and experimental data processing demonstrated an excellent performance of the techniques proposed, whose computational complexity is low enough to permit real-time implementation.

## ACKNOWLEDGMENT

The authors would like to thank Joshua Berlin for his generous assistance.

## REFERENCES

[1] M. Stojanovic and L. Freitag, "Multichannel detection for wideband underwater acoustic CDMA communications," *IEEE J. Ocean. Eng.*, vol. 31, no. 3, pp. 685–695, Jul. 2006.
[2] E. Calvo and M. Stojanovic, "Efficient channel-estimation-based multiuser detection for underwater CDMA systems," *IEEE J. Ocean. Eng.*, vol. 33, no. 4, pp. 502–512, Oct. 2008.
[3] C. He, J. Huang, and Z. Ding, "A variable-rate spread-spectrum system for underwater acoustic communications," *IEEE J. Ocean. Eng.*, vol. 34, no. 4, pp. 624–633, Oct. 2009.
[4] J. Ling, H. He, J. Li, W. Roberts, and P. Stoica, "Covert underwater acoustic communications," *J. Acoust. Soc. Amer.*, vol. 128, no. 5, pp. 2898–2909, 2010.

[5] S. Liu, G. Qiao, and A. Ismail, "Covert underwater acoustic communication using dolphin sounds," *J. Acoust. Soc. Amer.*, vol. 133, no. 4, pp. EL300–EL306, 2013.
[6] F. Qu, X. Qin, L. Yang, and T. Yang, "Spread-spectrum method using multiple sequences for underwater acoustic communications," *IEEE J. Ocean. Eng.*, vol. 43, no. 4, pp. 1215–1226, Oct. 2018.
[7] Y. M. Aval and M. Stojanovic, "Differentially coherent multichannel detection of acoustic OFDM signals," *IEEE J. Ocean. Eng.*, vol. 40, no. 2, pp. 251–268, Apr. 2015.
[8] A. Tadayon and M. Stojanovic, "Low-complexity superresolution frequency offset estimation for high data rate acoustic OFDM systems," *IEEE J. Ocean. Eng.*, vol. 44, no. 4, pp. 932–942, Oct. 2019.
[9] A. Tadayon and M. Stojanovic, "Iterative sparse channel estimation and spatial correlation learning for multichannel acoustic OFDM systems," *IEEE J. Ocean. Eng.*, vol. 44, no. 4, pp. 820–836, Oct. 2019.
[10] D. N. Kalofonos, M. Stojanovic, and J. G. Proakis, "Performance of adaptive MC-CDMA detectors in rapidly fading Rayleigh channels," *IEEE Trans. Wireless Commun.*, vol. 2, no. 2, pp. 229–239, Mar. 2003.
[11] P. van Walree, E. Sangfelt, and G. Leus, "Multicarrier spread spectrum for covert acoustic communications," in *Proc. OCEANS*, 2008, pp. 1–8.
[12] G. Leus and P. van Walree, "Multiband OFDM for covert acoustic communications," *IEEE J. Sel. Areas Commun.*, vol. 26, no. 9, pp. 1662–1673, Dec. 2008.
[13] Z. Wang, S. Zhou, J. Catipovic, and P. Willett, "Asynchronous multiuser reception for OFDM in underwater acoustic communications," *IEEE Trans. Wireless Commun.*, vol. 12, no. 3, pp. 1050–1061, Mar. 2013.
[14] N. Iruthayanathan, K. S. Vishvaksenan, and V. Rajendran, "Performance of spread spectrum based multi-carrier system in underwater communication using transmitter pre-processing," *IEEE Access*, vol. 4, pp. 5128–5134, 2016.
[15] D. Egnor, L. Cazzanti, J. Hsieh, and G. S. Edelson, "Underwater acoustic single- and multi-user differential frequency hopping communications," in *Proc. IEEE OCEANS Conf.*, 2008, pp. 1–6.
[16] G. Qiao, S. Xing, and F. Zhou, "A multi-user detection scheme based on polar code construction in downlink underwater acoustic OFDM communication system," *IEEE Access*, vol. 7, pp. 65973–65981, 2019.
[17] Y. V. Zakharov and A. K. Morozov, "OFDM transmission without guard interval in fast-varying underwater acoustic channels," *IEEE J. Ocean. Eng.*, vol. 40, no. 1, pp. 144–158, Jan. 2015.
[18] Z. Li and M. Stojanovic, "Spread-spectrum multi-carrier communication in interference-limited acoustic regimes," in *Proc. Underwater Acoust. Conf. Exhibit.*, 2019, pp. 1–6.
[19] Z. Li and M. Stojanovic, "Multi-user multi-carrier underwater acoustic communications," in *Proc. Global Oceans 2020: Singapore—U.S. Gulf Coast*, 2020, pp. 1–4.
[20] R. Gallager, "Low-density parity-check codes," *IRE Trans. Inf. Theory*, vol. 8, no. 1, pp. 21–28, 1962.
[21] D. J. MacKay and R. M. Neal, "Good codes based on very sparse matrices," in *Proc. IMA Int. Conf. Cryptography Coding*, 1995, pp. 100–111.
[22] A. Cassagne et al., "AFF3CT: A fast forward error correction toolbox!," *Elsevier SoftwareX*, vol. 10, 2019, Art. no. 100345.
[23] J. Zhang and M. Fossorier, "Shuffled iterative decoding," *IEEE Trans. Commun.*, vol. 53, no. 2, pp. 209–213, Feb. 2005.
[24] A. Viterbi, "An intuitive justification and a simplified implementation of the MAP decoder for convolutional codes," *IEEE J. Sel. Areas Commun.*, vol. 16, no. 2, pp. 260–264, Feb. 1998.
[25] E. Arikan, "Channel polarization: A method for constructing capacity-achieving codes for symmetric binary-input memoryless channels," *IEEE Trans. Inf. Theory*, vol. 55, no. 7, pp. 3051–3073, Jul. 2009.
[26] B. Li, H. Shen, and D. Tse, "An adaptive successive cancellation list decoder for polar codes with cyclic redundancy check," *IEEE Commun. Lett.*, vol. 16, no. 12, pp. 2044–2047, Dec. 2012.
[27] *5G; NR; Multiplexing and Channel Coding*, Tech. Specification 38.212, 3rd Gener. Partnership Project, Version 15.2.0, Jun. 2018.
[28] I. Tal and A. Vardy, "List decoding of polar codes," *IEEE Trans. Inf. Theory*, vol. 61, no. 5, pp. 2213–2226, May 2015.
[29] M. B. Porter, *The BELLHOP Manual and User's Guide: Preliminary Draft*. La Jolla, CA, USA: Heat, Light, and Sound Research, Inc., 2011.
[30] P. Qarabaqi and M. Stojanovic, "Statistical characterization and computationally efficient modeling of a class of underwater acoustic communication channels," *IEEE J. Ocean. Eng.*, vol. 38, no. 4, pp. 701–717, Oct. 2013.
[31] D. A. Cuji, Z. Li, and M. Stojanovic, "ACT: An acoustic communications testbed," in *Proc. IEEE Conf. Comput. Commun. Workshops*, 2022, pp. 1–6.